# ENERGY FLOWS IN AN ORIFICE PULSE TUBE REFRIGERATOR*

W. Rawlins, R. Radebaugh, P.E. Bradley
National Institute of Standards and Technology, Boulder, CO 80303

K.D. Timmerhaus
University of Colorado, Department of Chemical Engineering
Boulder, CO 80309

## ABSTRACT

A technique which allows for the instantaneous measurements of mass flow rate and temperature in an orifice pulse tube refrigerator (OPTR) during actual operation has been developed recently. This paper presents the values of enthalpy, entropy, and work fluxes at the cold end of the pulse tube evaluated from these measurements. They are thermodynamically self consistent within 1%. An analytical model describing the operation of an OPTR was developed at the National Institute of Standards and Technology (NIST) in the late 1980's. This model assumes adiabatic performance of the pulse tube and purely sinusoidal mass flow rates, temperature, and pressure oscillations in the OPTR. The experimentally measured enthalpy flux varies from 60% to 85% of that predicted by the adiabatic model. The experimental work reported here also gives values for various phase relationships that are needed for some calculations with the analytical model.

## INTRODUCTION

In the late 1980's Radebaugh and co-workers[1] at the National Institute of Standards and Technology (NIST) developed a simple analytical model of the orifice pulse tube refrigerator (OPTR). In this model compression and expansion within the pulse tube were assumed to be adiabatic and pressure, mass flow rate, and temperature were assumed to vary sinusoidally. The first law of thermodynamics was used to show that the gross refrigeration power of a pulse tube refrigerator is given by the time-averaged enthalpy flow $\langle \dot{H} \rangle$ within the pulse tube. In the NIST analytical model for sinusoidal behavior this average enthalpy flow is

$$\langle \dot{H} \rangle = \frac{1}{2} C_p \dot{m}_1 T_1 \cos\phi \,, \qquad (1)$$

*Research sponsored by NASA/Ames Research Center. Contribution of NIST, not subject to copyright.

*Advances in Cryogenic Engineering*, Vol. 39,
Edited by P. Kittel, Plenum Press, New York, 1994

where $\dot{m}_1$ and $T_1$ are the amplitudes of the sinusoidal oscillations of the mass flow rate and temperature, and $\phi$ is the phase angle between them. With the adiabatic assumption, $\langle \dot{H} \rangle$ is related to the pressure by the equation[1]

$$\langle \dot{H} \rangle = \langle \dot{V} P_D \rangle = \frac{1}{2} R\, T_h\, \dot{m}_{o,1}\, P_1 / P_0 , \tag{2}$$

where $\langle \dot{V} P_D \rangle$ is the hydrodynamic work flow rate $\langle \dot{W}_h \rangle$, $P_D$ is the dynamic pressure, $T_h$, is the temperature at the hot end of the pulse tube, $\dot{m}_{o,1}$ is the amplitude of the mass flow rate at the orifice, $P_1$ is the amplitude of the pressure oscillation, $P_o$ is the average pressure, and $R$ is the ideal gas constant per unit mass for helium. The mass flow rate and the dynamic pressure at the warm end of the pulse tube are relatively easy quantities to measure.

The NIST analytical model showed that $\dot{m}_{o,1}$ was related to the volume $V_t$ of the pulse tube by

$$\dot{m}_{o,1} = \frac{|\dot{P}|\, V_t}{\gamma\, R\, T_h \tan\theta} = \frac{2\pi f P_1 V_t}{\gamma\, R T_h \tan\theta} , \tag{3}$$

where $\dot{P}$ is the time rate of change of the pressure, $\gamma$ is the ratio of specific heats, $\theta$ is the phase angle between the mass flow rates at the two ends of the pulse tube and $f$ is the frequency. Equations (2) and (3) can be used to calculate the gross refrigeration power for a given size pulse tube if $\theta$ is known. We report here on measurements of $\theta$ in an actual pulse tube refrigerator to provide useful design information.

The calculation of $\langle \dot{H} \rangle$ in a real pulse tube is difficult because of various losses within the pulse tube that are not very well understood. One of the losses is associated with the instantaneous heat transfer between the gas and the tube walls. This loss associated with nonadiabatic behavior can be calculated if the flow is laminar. However, the loss associated with large scale turbulence resulting from entrance effects and the loss associated with streaming[2] are very difficult to calculate and have not been done to date. These losses result in an irreversible generation of entropy along the pulse tube which can reduce $\langle \dot{H} \rangle$ below its ideal adiabatic value.

In this paper we present experimental results for $\langle \dot{H} \rangle$ within a pulse tube and compare them to the analytical model. We also present experimental results for the time-averaged entropy flow $\langle \dot{S} \rangle$ and the time-averaged hydrodynamic work flow $\langle \dot{W}_h \rangle$ within the pulse tube. The relationship between these quantities is found by starting with the thermodynamic relation

$$dh = vdP + Tds . \tag{4}$$

By using the dynamic pressure $P_D$ for the differential $dP$, Eq. (3) is then integrated, multiplied by $\dot{m}$, and averaged over a cycle to obtain

$$\langle \dot{H} \rangle = \langle \dot{V} P_D \rangle + T_o \langle \dot{S} \rangle , \tag{5}$$

where $T_o$ is the average temperature. The first term on the right side of Eq. (2) is the time-averaged hydrodynamic work flow $\langle \dot{W}_h \rangle$. In an ideal pulse tube where compression and expansion are perfectly adiabatic, there is no entropy change throughout the cycle. Thus, $\langle \dot{S} \rangle = 0$, and $\langle \dot{H} \rangle = \langle \dot{W}_h \rangle$, in the ideal pulse tube. In a real pulse tube the losses discussed earlier give rise to a negative value of $\langle \dot{S} \rangle$; that is, the entropy flows toward the compressor. In that case $\langle \dot{H} \rangle / \langle \dot{W}_h \rangle < 1$.

ons of the mass flow rate and
e adiabatic assumption, $\langle \dot{H} \rangle$ is

(2)

he dynamic pressure, $T_h$, is the
ide of the mass flow rate at the
average pressure, and $R$ is the
and the dynamic pressure at the
asure.
o the volume $V_t$ of the pulse tube

(3)

of specific heats, θ is the phase
lse tube and $f$ is the frequency.
tion power for a given size pulse
actual pulse tube refrigerator to

because of various losses within
ne losses is associated with the
alls. This loss associated with
However, the loss associated with
ss associated with streaming[2] are
se losses result in an irreversible
$\dot{S}$⟩ below its ideal adiabatic value.
within a pulse tube and compare
lts for the time-averaged entropy
$\dot{W}_h$⟩ within the pulse tube. The
the thermodynamic relation

(4)

(3) is then integrated, multiplied

(5)

right side of Eq. (2) is the time-
se tube where compression and
ge throughout the cycle. Thus,
l pulse tube the losses discussed
py flows toward the compressor.

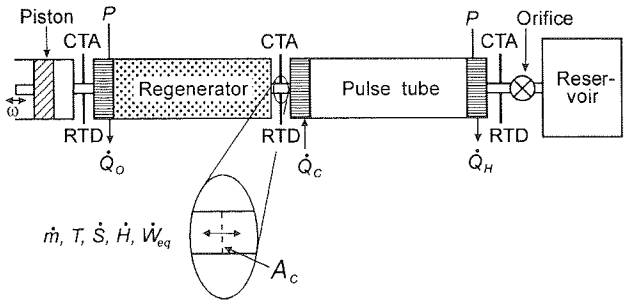


**Figure 1** Schematic of an orifice pulse tube refrigerator.

## EXPERIMENTAL METHODS

A schematic of an OPTR is shown in Fig. 1. In this figure CTA indicates locations for constant temperature anemometers where measurements of the mass flow rate were made, RTD indicates locations for resistance temperature detectors where a measurements of temperature were made, $\dot{Q}$ represents heat transfer in the directions indicated by the arrows, ω is the angular frequency of oscillation of the compressor, $P$ is the pressure, $\dot{m}$ is the mass flow rate, $T$ is the temperature, $\dot{S}$ is the rate of entropy generation, $\dot{H}$ is the rate of enthalpy flow, and $\dot{W}_h$ is the hydrodynamic work flow rate.

As indicated in Fig. 1, measurements of the mass flow rate and temperature are made at the cold end of the regenerator and not within the pulse tube. The pressure at that location is assumed to be the same as that measured at the warm end of the pulse tube. As shown in Fig. 1, a heat exchanger at the cold end of the pulse tube is located between the CTA and RTD sensors and the pulse tube. According to the first law of thermodynamics, the time-averaged enthalpy flow $\langle \dot{H} \rangle_{pt}$ within the pulse tube is given by

$$\langle \dot{H} \rangle_{pt} = \langle \dot{H} \rangle_{reg} + \dot{Q}_c , \tag{6}$$

where $\langle \dot{H} \rangle_{reg}$ is the time-averaged enthalpy flow at the cold end of the regenerator and $\dot{Q}_c$ is the heat flow into the cold end heat exchanger. In the measurements reported here, there was no net heat input to this heat exchanger. Thus the only heat input would be that conducted down the pulse tube, which is only a few percent of $\langle \dot{H} \rangle$. We have therefore assumed that $\langle \dot{H} \rangle_{reg} = \langle \dot{H} \rangle_{pt}$. Because of the small volume associated with the heat exchanger and because of the excellent heat transfer within it, we have also assumed that there is no entropy generation within that section, nor any loss of hydrodynamic work flow within that section. Thus, the derived values of $\langle \dot{S} \rangle$ and $\langle \dot{W}_h \rangle$ from the cold end of the regenerator are approximately equivalent to those within the cold end of the pulse tube.

Rawlins recently has adapted constant temperature anemometers[3,4] (CTA) and resistance temperature detectors[5] (RTD) to measure instantaneous mass flow rates and temperatures during actual operation of an OPTR. Constant temperature anemometry infers the mass flow rate of a fluid by measuring the heat transfer rate from a resistively heated element.[6] These sensors can have response times as short as several microseconds. Resistance temperature detectors monitor the change of resistance for a resistive element with respect to changing temperature. In the configuration used in this study, both the CTA and RTD were identically constructed from 2 mm lengths of 3.8 μm diameter tungsten wire suspended in the fluid stream by stiff wire supports. The supports were electrical conductors and also served as the electrical connections for the sensors. The CTA was operated at approximately 200 K warmer than the surrounding fluid. Conversely, the RTD was operated with as little resistive heating as possible. Both sensors were placed inside the 3 mm tubing between the cold ends of the regenerator and pulse tube and inside

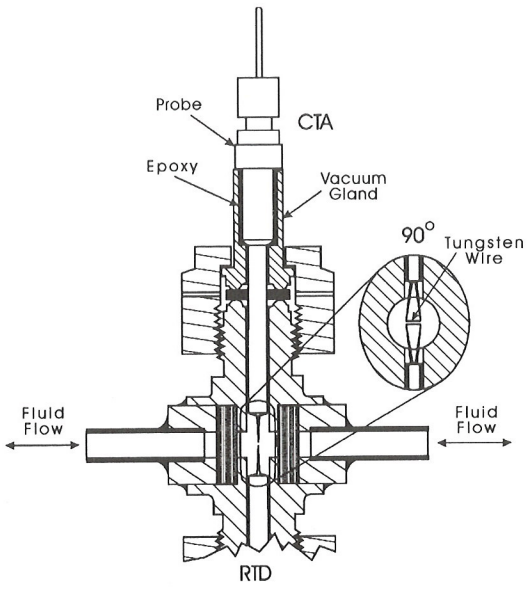


**Figure 2** Schematic depicting modified vacuum gland with CTA and RTD probes placed perpendicular to the flow of the fluid.

the 4.75 mm tubing at the warm ends of the regenerator and pulse tube (Figs. 1 and 2). The response times of the CTA and RTD in this system, with only free convection, were approximately 20 μs and 260 μs, respectively.

The small size of the sensors allowed them to be placed in a relatively confined environment. The tungsten wire proved to be very durable and resisted breakage during the rapid mass flow reversals that take place in an OPTR at both cryogenic and room temperatures. The small size of these sensors only minimally disturbed the OPTR operation and allowed instantaneous measurements to be made of the mass flow rates and temperatures during actual operation. The regenerators used in these experiments were constructed from a stainless steel tube having a length of 122 mm, a diameter of 18.88 mm, and a wall thickness of 0.31 mm. This tube was packed with circular disks punched from a woven stainless steel cloth of 200x200 mesh, a combination of 3 meshes (250x250, 200x200, and 150x150) used in a graded fashion, or a calendered form of the 200x200 mesh. The porosity of the first two regenerators was 0.65 and the third was 0.55. The pulse tube was constructed from a stainless steel tube having a length of 122 mm, a diameter of 9.525 mm, and a wall thickness of 0.254 mm. The reciprocating compressor used to supply the work input to the OPTR had a displacement of 25 $cm^3$.

## RESULTS

Figure 3 shows an example of the mass flow rates measured at the three locations shown in Fig. 1 for an OPTR operating at 15 Hz. The mass flow rate and gas temperature at the cold end of the regenerator are plotted In Fig. 4 for the same operating conditions. Figures 3 and 4 demonstrate that the mass flow and temperature oscillations in the system being studied were not sinusoidal. Furthermore, even though the total mass which flows past the sensor in the positive direction (away from the compressor) is equal to that in the negative direction (towards the compressor), the peak flows and half-cycle frequencies are not equivalent. Figure 4 demonstrates that the phase relationship between the mass flow rate and temperature changes between the two half-cycles. Therefore, the experimentally measured phase angles were averaged between the two half-cycles. The time averaged enthalpy flow at the cold end of the regenerator is the regenerator loss. For an ideal gas the average enthalpy flow is given by[1]


th CTA and RTD probes

ulse tube (Figs. 1 and 2). The
convection, were approximate-

laced in a relatively confined
sisted breakage during the rapid
ic and room temperatures. The
OPTR operation and allowed
and temperatures during actual
nstructed from a stainless steel
l a wall thickness of 0.31 mm.
stainless steel cloth of 200x200
x150) used in a graded fashion,
first two regenerators was 0.65
a stainless steel tube having a
thickness of 0.254 mm. The
OPTR had a displacement of

red at the three locations shown
and gas temperature at the cold
ng conditions. Figures 3 and 4
e system being studied were not
s past the sensor in the positive
negative direction (towards the
uivalent. Figure 4 demonstrates
erature changes between the two
s were averaged between the two
he regenerator is the regenerator

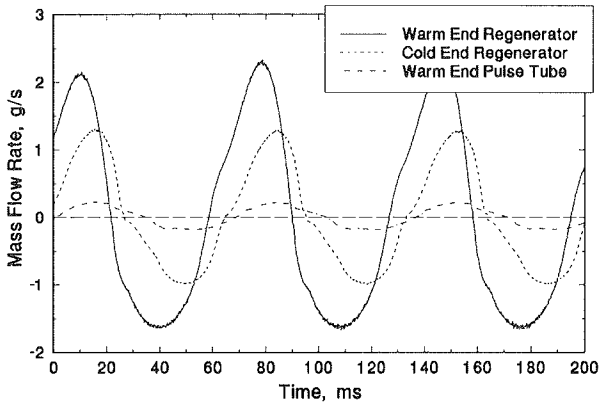


**Figure 3** Mass flow rates as a function of time as measured at various locations in an orifice pulse tube refrigerator during operation at 15 Hz.

$$\langle \dot{H} \rangle = \frac{C_p}{\tau} \oint \dot{m} T \, dt, \tag{7}$$

where $C_p$ is the heat capacity at constant pressure and $\tau$ is the time required to complete one cycle. If sinusoidal behavior is assumed for the mass flow and temperature, Eq. (7) is identical to Eq. (1). Equation (7) was used to numerically calculate the actual average enthalpy flow from the experimental data which was then compared to the value predicted using the sinusoidal approximation in Eq. (1). To evaluate the enthalpy flux from Eq. (1), average values for $\phi$, $T_1$, and $\dot{m}_1$ were determined from the experimental data. A plot comparing the results is shown in Fig. 5. Note that the sinusoidal approximation to the meaasured data consistently predicts a higher enthalpy flux than that measured experimentally.

Radebaugh[1] has also used the analytical model to calculate the refrigeration power per unit flow rate at the cold end. This calculation requires the phase angle between the mass flow rates at the cold and warm end of the pulse tube be known. He also indicates that 30° is a good choice for this angle. The average experimentally determined value was 25.6° with a standard deviation of 3.8°. Other phase angle relations also evaluated included that between the mass flow rate and pressure at the warm end of the pulse tube of 19.3° with a standard deviation of 6.2°, and that between the mass flow rate and temperature at the cold end of the pulse tube of 17.6° with a standard deviation of 7.7°.

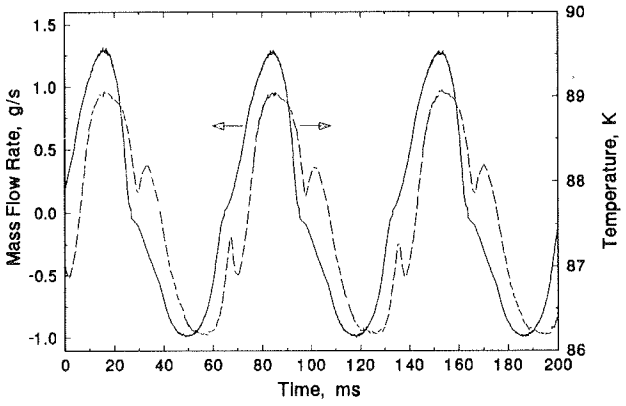


**Figure 4** Plot of the mass flow rate and temperature as functions of time at the cold end of the pulse tube operating at 15 Hz.

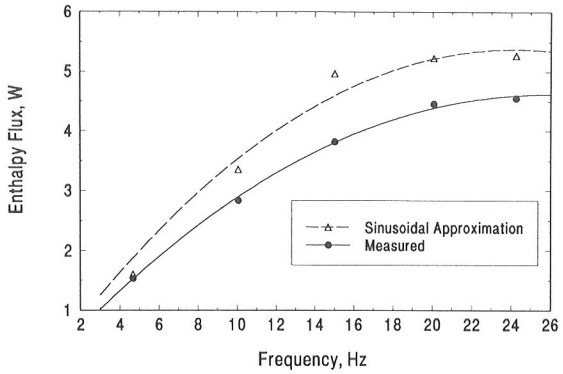


**Figure 5** Plot of the measured and sinusoidally approximated enthalpy flux as a function of frequency.

**Table 1** Average fluxes and relative error at the cold end of the pulse tube

| Frequency (Hz) | $\langle \dot{m} \rangle$ (g/s) | $\langle \dot{H} \rangle$ (W) | $T_o \langle \dot{S} \rangle$ (W) | $\langle \dot{W}_h \rangle$ (W) | $E_r$ |
|---|---|---|---|---|---|
| 10.07 | 0.519 | 2.528 | -1.267 | 3.802 | 0.0018 |
| 10.07 | 0.510 | 2.514 | -1.195 | 3.713 | 0.0012 |
| 15.06 | 0.706 | 3.267 | -1.303 | 4.556 | -0.0030 |
| 20.25 | 0.789 | 3.567 | -1.061 | 4.646 | 0.0038 |
| 24.17 | 0.804 | 3.644 | -0.925 | 4.594 | 0.0056 |

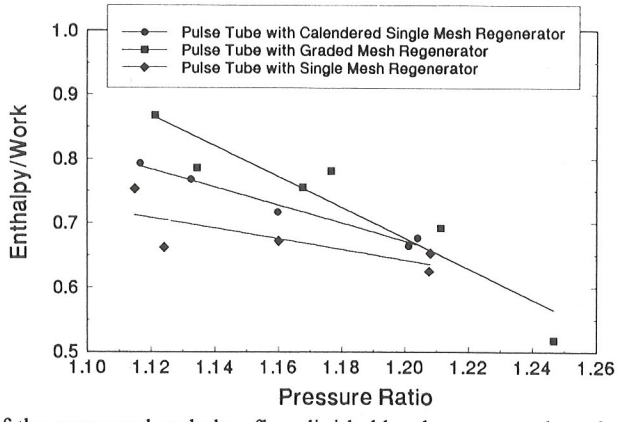


**Figure 6** Plot of the measured enthalpy flux divided by the measured work as a function of the presssure ratio in the pulse tube.

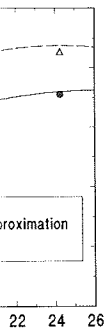


enthalpy flux as a function of

of the pulse tube

| $\langle \dot{W}_h \rangle$ (W) | $E_r$ |
|---|---|
| 3.802 | 0.0018 |
| 3.713 | 0.0012 |
| 4.556 | -0.0030 |
| 4.646 | 0.0038 |
| 4.594 | 0.0056 |

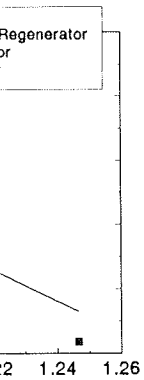


easured work as a function of

The hydrodynamic work term in Eq. (5) was evaluated by using the ideal gas law to determine the volume flow rate. This resulted in

$$\langle \dot{W}_h \rangle = \langle \dot{V} P_D \rangle = \frac{R}{\tau} \oint \frac{T P_D \dot{m}}{P} \, dt \,, \tag{8}$$

where all the values inside the integral are instantaneous quantities. The dynamic pressure $P_D$ is the difference between the actual pressure in the pulse tube and the average pressure of the pulse tube. Equation (8) was evaluated numerically using the instantaneous values of these parameters. Table 1 shows the results for a series of experiments for values of $T_o\langle \dot{S} \rangle$, $\langle \dot{H} \rangle$, and $\langle \dot{W}_h \rangle$. From Eq. (5) we define a relative residual error $E_r$ as

$$E_r \equiv \frac{(\langle \dot{H} \rangle - \langle \dot{W}_h \rangle - T_o \langle \dot{S} \rangle)}{\langle \dot{W}_h \rangle} \,. \tag{9}$$

In all cases the error is less than 1%. According to Eq. (5), $E_r = 0$. The experimental values of $E_r$ indicate the degree of thermodynamic self consistency within the data. These experimental values are given in the last column of Table 1.

The ratio of the average enthalpy flux to the average hydrodynamic work flow is an important parameter. For the ideal pulse tube where the gas undergoes adiabatic processes there is no entropy flow, and according to Eq. (5), $\langle \dot{H} \rangle_{id} = \langle \dot{W}_h \rangle$. Thus, the ratio $\langle \dot{H} \rangle / \langle \dot{W}_h \rangle$ indicates the relative performance of an actual pulse tube to the ideal pulse tube. Figure 6 shows this measured ratio for the case of a single pulse tube, but with three different regenerators. Ideally, the regenerator should not affect the enthalpy flow in the pulse tube. In practice each regenerator can introduce slightly different entrance effects on the pulse tube. Figure 6 indicates there is little difference with the three different regenerators. For low pressure ratios the enthalpy flow is about 80% of what the ideal adiabatic model calculates, but it decreases to about 60% at higher pressure ratios. The value of $\langle \dot{W}_h \rangle$ was also evaluated at the warm end of the pulse tube. The ratio of $\langle \dot{W}_h \rangle$ at the warm end to the cold end of the pulse tube was 0.85 with a standard deviation of 0.0067. This reduction of $\langle \dot{W}_h \rangle$ at the warm end is a result of losses within the pulse tube.

## CONCLUSION

Measurements of instantaneous mass flow rates, temperature, and pressure have been made on an OPTR during actual refrigerator operation. These measurements have allowed enthalpy, entropy, and work flows to be determined experimentally as well as the phase angle relationships between oscillating parameters in this system. These results will aid in improving input parameters to the analytical model developed at NIST as well as verifying model predictions. The experimentally measured enthalpy flows within the pulse tube used here ranged from 60% to 85% of the ideal value from the NIST adiabatic model.

## REFERENCES

1. R. Radebaugh, A review of pulse tube refrigeration, in: "Advances in Cryogenic Engineering," Vol. 35, Plenum Press, New York (1990), p. 1191.
2. J. Lee, R. Radebaugh, P. Kittel, and K.D. Timmerhaus, Flow patterns intrinsic to the pulse tube refrigerator, in: "Proceedings of the 7th International Cryocooler Conference," (1993), p. 125.

3. W. Rawlins, R. Radebaugh, K.D. Timmerhaus, Thermal anemometry for mass flow measurement in oscillating cryogenic gas flows, Rev. Sci. Instrum. (1993), to be published.
4. W. Rawlins, "The Measurement and Modeling of Regenerator Performance in an Orifice Pulse Tube Refrigerator," Ph.D. thesis, University of Colorado, Boulder (1992).
5. W. Rawlins, R. Radebaugh, W., K.D. Timmerhaus, Resistance thermometers with fast response for use in rapidly oscillating gas flows, in: "Temperature; Its Measurement and Control in Science and Industry," Vol. 6, Part 1, American Institute of Physics (1992), p. 471.
6. A. E.Perry, Hot Wire Anemometry, Clarendon Press, Oxford, (1982).